Published in final edited form as:

J Am Soc Mass Spectrom. 2016 September ; 27(9): 1476–1482. doi:10.1007/s13361-016-1423-z.

CO_2 cluster ion beam, an alternative projectile for secondary ion mass spectrometry

Hua Tian[1], **Dawid Maciążek**[2], **Zbigniew Postawa**[2], **Barbara J. Garrison**[1], and **Nicholas Winograd**[1]

[1]Chemistry Department, The Pennsylvania State University, University Park, PA 16802, USA
[2]Smoluchowski Institute of Physics, Jagiellonian University, ulica Lojasiewicza 11, 30 - 348 Krakow, Poland

Abstract

The emergence of argon - based gas cluster ion beams for SIMS experiments opens new possibilities for molecular depth profiling and 3D chemical imaging. These beams generally leave less surface chemical damage and yield mass spectra with reduced fragmentation when compared to smaller cluster projectiles. For nanoscale bioimaging applications, however, limited sensitivity due to low ionization probability and technical challenges of beam focusing remain problematic. The use of gas cluster ion beams based upon systems other than argon offer an opportunity to resolve these difficulties. Here we report on the prospects of employing CO_2 as a simple alternative to argon. Ionization efficiency, chemical damage, sputter rate and beam focus are investigated on model compounds using a series of CO_2 and Ar cluster projectiles (cluster size 1000~5000) with the same mass. The results show that the two projectiles are very similar in each of these aspects. Computer simulations comparing the impact of Ar_{2000} and $(CO_2)_{2000}$ on an organic target also confirm that the CO_2 molecules in the cluster projectile remain intact, acting as a single particle of m/z 44. The imaging resolution employing CO_2 cluster projectiles is improved by more than a factor of 2. The advantage of CO_2 vs Ar is also related to the increased stability which, in addition, facilitates the operation of the GCIB system at lower backing pressure.

Graphical abstracts

Address reprint requests to Hua Tian, 215 Chemistry Building, University Park, State College, PA 16802, Phone: (814) 876 - 2878, fax: (814) 863 - 0618 hut3@psu.edu.

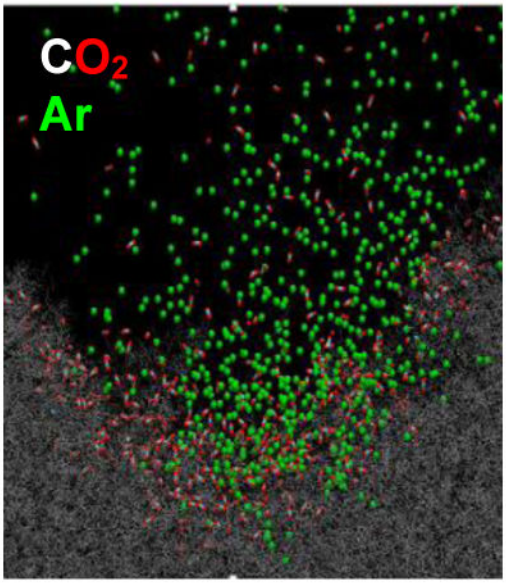

Introduction

The incorporation of cluster ion beams for molecular desorption in Secondary Ion Mass Spectrometry (SIMS) has quickly transformed the field. These species reduce the fragmentation associated with atomic ion projectiles yielding cleaner mass spectra [1]. Moreover, since there is generally less chemical damage accumulation during the bombardment process, molecular depth profiling is now routinely possible [2–5]. There are a plethora of projectiles under study ranging from small metal cluster ions produced from a liquid metal ion gun (LMIG) to gas cluster ion beams (GCIB) produced via supersonic expansion. The LMIG ions are easily focused to a sub - 100 nm spot size and are generally used for imaging studies [6–9]. The GCIB ions are not easily focused, but have been utilized in a dual beam environment for removing residual damage accumulation left by the analyzing beam, resulting in improved molecular depth profiling [5, 10]. A tightly focused Ar_{1000}^{+} cluster ion beam has been reported to imaging organic grid with ~4 μm beam diameter [11]. Another popular ion source utilizes C_{60}^{+} ions. This source represents a good compromise between the LMIG and the GCIB sources since the secondary molecular ion intensity is generally higher than that obtained with the LMIG sources, and a 300 nm spot size can be achieved for imaging [12–14]. At this time, the use of the GCIBs for SIMS is limited due to spot - size considerations and to the fact that ionization probability is usually poor when employing the larger clusters [15, 16].

Due to the promising attributes of GCIBs, there is active research aimed toward improving both ionization and focusing properties. There are many options, in addition to the commonly employed Ar_n^{+}, with n = 1000 – 10000, since the clusters are formed by supersonic expansion of a gas or gas mixture followed by electron impact ionization. Hence, the chemical or physical properties of the gas molecules can be selected from a wide range of volatile materials. One interesting approach is to employ water vapor as the gas, yielding

$[H_2O]_n^+$ clusters. The idea is to bring protons to the impact site in order to enhance the yield of $[M + H]^+$ ions. Increases of more than 10× in ionization efficiency relative to Ar_n^+ have been reported for a range of molecules [17, 18]. Similarly, our laboratory has reported that incorporation of 2~3% CH_4 and 5% HCl into Ar_n^+ also increases the $[M + H]^+$ yield, although not quite as much as the $[H_2O]_n^+$ beam [19, 20]. In addition, there is evidence that CO_2 - seeded Ar GCIB's are easier to focus presumably due to better chromaticity in the focusing lenses [21, 22].

Here we propose the use of a GCIB formed from CO_2 gas as an improved primary ion source for SIMS acquisition and imaging. This approach offers a number of potential advantages since CO_2 clusters are nearly 4 times as stable as Ar clusters due to stronger van der Waals interaction. This increased stability means that it is experimentally easier to produce larger clusters, and that these clusters are less prone to metastable decay as they travel down the ion beam column. To establish the efficacy of a CO_2 - GCIB, we show that for clusters ranging from 1000 to 5000 molecules at 20 keV acceleration energy, there is no observable bond - breaking of CO_2 molecules and that the projectile acts very much like a cluster of particles of *m/z* 44 rather than *m/z* 40. We demonstrate this point with computer simulations, sputtering yield measurements and mass spectral comparisons using a series of reference compounds. Moreover, imaging resolution using the CO_2 - GCIB is improved by more than a factor of two versus employing the Ar - GCIB, and the backing pressure necessary to create a specific - sized cluster is also reduced by more than a factor of two.

Experimental

Sample preparation

1,2 - dihexadecanoyl - *sn* - glycero - 3 - phosphocholine (DPPC) and N - palmitoyl - D - *erythro* - sphingosylphosphorylcholine (SM d18:1/16:0) were prepared as thin films using a Langmuir - Blodgett (LB) trough. The LB films were prepared using a Kibron μTrough XS (Kibron, Inc., Helsinki, Finland). Distilled and de - ionized water (Milli - Q purified, with a resistance of 18.2 mΩ·m) was employed as the sub - phase. To prepare the films, 7 μL of a solution of either DPPC or SM (2 mg/mL dissolved in chloroform) was applied to the air - water interface and solvent was allowed to evaporate for 15 min. The lipid monolayer was compressed at a rate of 4 – 6 $Å^2$/chain/min through the gas - liquid phase transition. Deposition of the monolayer onto piranha - etched Si substrates occurred at a constant surface pressure of 30 mN/m and a deposition rate of 2 nm/min. Films were allowed to air dry for 30 min before transfer into a desiccator until SIMS characterization.

Trehalose films were prepared by spin - coating of trehalose solution onto a Si substrate. D - (+) - trehalose dehydrate (BioReagent, Sigma) was dissolved into HPLC water at the concentration of 0.1 M and 0.5 M. An aliquot of 50 μL of the 0.1 M solution was spin - coated (Laurell, WS - 650MZ - 23NPP/UD2) onto a pre - cleaned silicon wafer (sonicated in chloroform, HPLC water and methanol for 5 min respectively) at 4000 rpm, resulting in a uniform thin film of ~20 nm in thickness [23]. A thicker film of ~100 nm thickness was prepared by spin - coating 100 μL of a 0.5 M solution onto the pre - cleaned silicon wafer.

The rubrene (≥98%, Sigma) coated London - 135 finder grid (Fisher Scientific, US) was prepared by submerging the grid into 0.2 mL rubrene solution (in chloroform, 0.1 M), followed by air drying.

SIMS characterization

To compare the behavior of SIMS spectra resulting from Ar_n^+ and $(CO_2)_n^+$ cluster bombardment, a series of projectiles was employed to interrogate the control samples. Various cluster sizes were examined with kinetic energy varied from 0.08 to 0.5 eV/nucleon, the values representative of typical SIMS experiments [3]. At 20 keV acceleration energy, these values correspond to Ar_n^+ clusters consisting of 5000, 4000, 3000, 2000 and 1000 atoms and $(CO_2)_n^+$ clusters consisting of 4575, 3689, 2752, 1831, and 923, molecules, respectively. The cluster sizes were selected using a Wien filter on the ion beam column which has a mass resolution of m/Δm ~5 and a Gaussian distribution ± 500~900 particles. This spread might cause a certain degree of overlap of the adjacent clusters, however, the majority of the cluster will be centered at the desired size. All measurements were performed on a J105 3D Chemical Imager (Ionoptika, Southampton, UK) as described elsewhere [24]. The cluster ion beam was directed to the sample at an angle of incidence of 45º.

Six parallel analyses were acquired for each cluster projectile on the DPPC, SM and trehalose films from fresh areas of the sample surface. To avoid the bias induced by the quadrupole transmission variation with mass [24], each acquisition was performed at maximum high mass (*m/z* 600~800) transmission first and then at optimized low mass (*m/z* 100~300) transmission from the same area. The primary ion dose was 10^{11} ions/cm^2 over an area of 200 × 200 μm^2 with 32 × 32 pixels for each acquisition. The selected high mass ions (H) and low mass ions (L) from DPPC, SM and trehalose were monitored to compare the H/L mass ratio, as well as the secondary ion yields.

Sputter rates were further compared between Ar_{2000}^+ and $(CO_2)_{1831}^+$ clusters though depth profiling of a thick trehalose film and by measuring the depth of the etch craters using an atomic force microscope (AFM) (NPX200, Selko Instruments Inc), which has the resolution in the Z and X/Y range are ca. 3 Å and 2 nm respectively. The primary ion dose for each sputter and analysis cycle is 2.5 × 10^{12} ions/cm^2 over an area of 200 × 200 μm^2 with 32 × 32 pixels.

The focus of the two beams was investigated by SIMS imaging of a rubrene coated London finder grid (135 mesh, Electron Microscopy Sciences, PA, US). Ar_n^+ and $(CO_2)_n^+$ beams with the same beam current, 17 pA were produced by adjust the grid and bending deflector, and then finely focused using an objective lens in the beam optics. Images were taken over an area of 500 × 500 μm^2 with 128 × 128 pixels at a dose of 2.9 × 10^{12} ions/cm^2.

Data processing

The SIMS data were processed using Ionoptika Image Analyser (Version: 1.0.8.14) to read the intensity of selected ions at a mass width of Δ*m/z* 0.5 for high mass ions (H) and of Δ*m/z* 0.2 for low mass ions (L). The H/L mass ratios and secondary ion yields were further determined for each standard film. A line scan across a SIMS image of a rubrene coated

London finder grid was performed using the protonated rubrene molecule $[M + H]^+$ at *m/z* 533.2 across a metal bar at the same area. Distances between 20% ~ 80% of maximum signal intensity were used to determine the beam sizes. The Nanopics1000 software was used to process the AFM data to determine the depth of the craters generated by Ar_{2000}^+ and $(CO_2)_{1831}^+$ clusters, respectively.

Computer Simulations

A detailed description of the molecular dynamics computer simulations used to model cluster bombardment can be found elsewhere [25]. Briefly, the motion of the particles is determined by integrating Hamilton's equations of motion. The forces among the particles are described by a blend of pair - wise additive and many - body potential energy functions. The atomistic ReaxFF - lg [26] potential splined with a ZBL potential [27] to properly describe high energy collisions is used to describe interactions among C and H atoms. The interactions between Ar atoms in the projectile and between Ar atoms and all other particles in the system are described by a Lennard - Jones potential splined with a KrC potential [28]. Since the experiments have been designed to be general for any substrate, a polystyrene sample (PS) used previously was chosen as the substrate. The polystyrene sample is composed from n - butyl - terminated polystyrene molecules. Each molecule contains 100 styrene repeat units or 1626 atoms. The sample was equilibrated to achieve the most optimal configurations for the used potentials by applying periodic boundaries and constant particle number, pressure and temperature conditions. The calculated atomic density of the equilibrated PS sample is 0.96 g/cm^3, which is close to the experimental density of 0.96 – 1.06 g/cm^3.

A hemispherical sample with diameter ~40 nm is cut - out after the equilibration procedure. The system contains 1,621,122 atoms or 997 molecules. Rigid and stochastic regions with a thickness of 0.7 and 2.0 nm, respectively, were used around the hemisphere to preserve the shape of the sample, and to simulate the thermal bath that keeps the sample at the required temperature and helps inhibit the pressure wave reflection from the system boundaries [29]. From an analysis of the binding forces associated with each projectile, we find that the calculated binding energy of the Ar cluster is 0.065 eV/atom, while the binding energy of the CO_2 cluster is 0.27 eV/molecule. These are average values, of course, since the binding energy of molecules at the surface of the cluster will be lower than those inside the projectile. Ar_{2000} and $(CO_2)_{2000}$ projectiles were used to bombard the crystal with a kinetic energy of 20 keV and an impact angle of 45°. These values were selected to reproduce the conditions used in the experimental studies as closely as possible. The geometrical diameters of the relaxed cluster projectiles are approximately 5.2, 5.4 and 5.6 nm for Ar_{2000}, $(CO_2)_{1831}$ and $(CO_2)_{2000,}$ respectively. Since it has been shown that the efficiency of a cluster sputtering process for organic materials only weakly depends upon the projectile impact point [30], only one impact was probed. The simulations are run at 0 K target temperature and extend up to 50 ps which is long enough to see a saturation in the sputtering yield vs time dependence. The calculations are performed with a LAMMPS code [31] that was modified for a more efficient modelling of sputtering phenomena.

Results and discussion

Relative secondary ion yields and fragmentation propensity of DPPC, SM and trehelose for a series of $(CO_2)_n^+$ and Ar_n^+ projectiles

The secondary ion yield ratios of selected ions generated by CO_2 and Ar cluster bombardment of the reference compounds are shown in Figure 1. Note that for DPPC (Figure 1a), the ratios are close to unity for both the protonated molecule $[M + H]^+$ at *m/z* 734 and for the fragment ions appearing at *m/z* 184 (phosphocholine) and 478 (monoglycerol phosphocholine). In general, the yield ratio is slightly greater than 1 when employing the smallest clusters and slightly less than 1 when employing the largest clusters. For SM (Figure 1b), examination of ions at *m/z* 125 (fragment $[C_2H_6PO_4]^+$), the fragment ion $[M - C_2H_4]^+$ at *m/z* 703 and the protonated molecule $[M + H]^+$ at *m/z* 731 yield similar behavior. For trehalose (Figure 1c), protonated molecules $[M + H]^+$ at *m/z* 343 and $[M + H - H_2O]^+$ fragments at *m/z* 325 exhibit similar trends. Only the protonated trehalose dimer $[2M + H]^+$ at *m/z* 685 exhibits a consistent yield ratio of less than 1.

To evaluate the fragmentation propensity of different projectiles, the H/L mass ratio of selected species from DPPC, SM and trehalose as a function of the kinetic energy per nucleon of the projectile are shown in Figure 2. In general, it is clear that the fragmentation patterns caused by Ar_n^+ and $(CO_2)_n^+$ bombardment are almost identical, regardless of cluster size over the explored range. As expected, for both Ar_n^+ and $(CO_2)_n^+$ clusters, the H/L mass ratios increase with cluster size in the range of 1000 to 5000, a trend observed by many other groups [1, 3, 15]. There are a few differences worthy of attention. For the DPPC film (Figure 2a), *m/z* 734/184 is slightly elevated using $(CO_2)_n^+$ compared with Ar_n^+, the enhancement is between 10~30% within the selected cluster size range. The ratio of two fragments, *m/z* 478/184, is roughly the same for both projectiles. We speculate that the larger $(CO_2)_n^+$ clusters exhibit slightly lower fragmentation than the corresponding Ar_n^+ cluster, although more experiments are necessary to prove this point. For the SM film (Figure 2b), the fragmentation behavior is identical for both projectiles within the limits of experimental error. For trehalose, the fragmentation patterns are very similar for both projectiles with one notable exception. Ar_n^+ shows 50% enhancement of *m/z* 707/325, which is the ratio of ion $[2M + Na]^+$ to $[M + H - H_2O]^+$. We have previously noted that the response of sodiated species can vary extensively, depending upon the nature of the projectile [20, 32]. Overall, the studies on these three model compounds suggest that the SIMS spectra associated with Ar_n^+ or $(CO_2)_n^+$ are closely aligned.

Sputter yield of Ar_{2000}^+ and $(CO_2)_{1831}^+$

A pair of clusters, Ar_{2000}^+ and $(CO_2)_{1831}^+$, were selected to determine the relative sputter yields. If our hypothesis that CO_2 is acting as a single particle of *m/z* 44 and hence should behave similarly to an atom of *m/z* 40 is correct, then the two yields should be quite similar. If the CO_2 molecule is dissociating or chemically reacting with the sample, we expect to see large differences in the two values.

Trehalose films were employed as the model system since this molecule forms smooth films of uniform thickness and has been employed extensively for molecular depth profiling

experiments using a variety of SIMS primary ions [33–35]. The intensity of the monitored ion, $[M + H – H_2O]^+$ at *m/z* 325, is plotted as a function of primary ion fluence for both projectiles in Figure 3. The depth profiling curves for Ar_n^+ are consistent with previous study using Ar_n^+ clusters of various sizes [36], with the notable exception that the interface width to the underlying substrate appears to be quite broad. From an AFM analysis of the eroded crater, also displayed in Figure 3, it is seen that this effect is due to a variation of the eroded depth, which is probably induced by a lateral inhomogeneity of the trehalose film thickness. The depth profile obtained with $(CO_2)_n^+$ shows a steadily increasing signal throughout the removal of the film instead of a steady state plateau, indicating either enhanced ionization or reduced fragmentation with increasing eroded depth. Although the depth resolution obtained with the CO_2 cluster beam appears to be better than that obtained with Ar_n^+, we suppose from the AFM profiles that this is caused by a better lateral homogeneity of the eroded crater.

From the AFM data, it is possible to convert the fluence scale to a depth scale, allowing estimation of the sputtering yield. Here, the yield for Ar_{2000}^+ is 64 ± 5 nm^3/particle, and 88 ± 10 nm^3/particle for $(CO_2)_{1831}^+$. These numbers are quite similar and hence support the notion that CO_2 is interacting with the surface as an intact molecule, behaving like an atom of *m/z* 44.

Computer simulations of Ar_{2000} and $(CO_2)_{2000}$ cluster bombardment

To further explore the difference between Ar_n^+ and $(CO_2)_n^+$ bombardment on a molecular level, computer simulations of the impact of both species have been carried out. The goal is to compare the properties of Ar_{2000} with $(CO_2)_{2000}$ when impacting onto an organic target at 20 keV energy and at an angle of incidence of 45º. Although these conditions are not identical to the experimental arrangement, the general aspects arising from the simulation should reveal any fundamental differences between the two clusters.

The evolution of the trajectories associated with each projectile is illustrated in Figure 4. Note that, qualitatively, the sputtering events and the formation of the crater occur at about the same time. Moreover, the crater sizes are virtually identical. From the simulations, we calculate that the yield of polystyrene monomer equivalents is 27.4 nm^3/projectile when employing Ar_{2000}^+, and 25.0 nm^3/projectile when employing $(CO_2)_{2000}^+$. These values are virtually identical, suggesting that the sputtering mechanism for the two projectiles is very similar. The difference in calculated yield for PS and the measured yield for trehalose is expected since the binding forces of the two systems are different, and the computer simulations utilize an unperturbed surface rather than the bombarded surface utilized in the experiments.

Finally, it is interesting to note that at the energy examined here, 0.25 eV per nucleon or 10 eV per molecule, no CO_2 molecules are dissociated during the impact event. There is simply not enough energy imparted to individual CO_2 molecules with a dissociation energy of >8 eV to break a significant number of bonds. Moreover, a detailed analysis of the two trajectories suggests that after 50 ps, ~5% of the CO_2 molecules are still interacting with the PS surface while none of the Ar atoms experience any attractive force. Given the kinetic

energy of these CO_2 molecules, however, it is unlikely that any of them will remain bound to the PS.

Imaging with Ar_{2000}^+ and $(CO_2)_{1823}^+$

As noted above, the CO_2 - based clusters are considerably more stable than their Ar - based counterparts. This property changes the conditions that are necessary for creating the beam in the laboratory. In general, the gas pressure used to create the supersonic expansion inside the GCIB source determines the size of the cluster. To achieve sizes in the 1000 – 10000 particle range, a backing pressure of up to 20 bar is required for Ar, while only 6~12 bar is required for CO_2. This reduced pressure not only reduces pumping requirements, but also reduces turbulence in the expansion chamber, which, in turn, yields a narrower cluster size distribution. Moreover, the increased stability of CO_2 should reduce the probability of metastable decay of the cluster as it travels down the ion beam column on the way to the sample surface [37].

To compare the beam focus of paired cluster projectiles, Ar_{2000}^+ and $(CO_2)_{1831}^+$, the finely focused beams with identical beam currents were used to image a rubrene coated London finder grid as shown in Figure 5. The total ion image using Ar_{2000}^+ shown in Figure 5 (a) appears to blur at the edge of the metal bar, while the image in Figure 5 (b) acquired using $(CO_2)_{1831}^+$ is much sharper. The signal intensity is shown in Figure 5 (c and d). The distance of 20~80% of the maximum signal (rubrene quasi - molecular ion at *m/z* 533.2) is 17 and 7 μm for Ar_{2000}^+ and $(CO_2)_{1831}^+$ respectively. We speculate that the reason for the improved beam focus is related to the feeding gas pressure, ~6 bar, in contrast to 20 bar required by the formation of Ar clusters. Consequently, turbulences and gas phase collisions during the supersonic expansion are reduced, resulting in a narrower distribution of cluster sizes as shown in Figure S 1, The distribution for $CO_2)_{1831}^+$ is 1831 ± 500, while 2000 ± 900 for Ar_{2000}^+, which demands a narrow energy range of focus lens that can be supplied by the current GCIB system. Another possibility is that the increased stability of CO_2 clusters reduces the probability of decomposition as the cluster travels down the ion beam column.

Conclusion and outlook

Here we examine the possibility of employing a pure CO_2 cluster as a source for SIMS imaging experiments by comparing ionization, fragmentation, yield and focusing properties to an argon cluster of similar mass. The results show that the two projectiles are very similar in each of these aspects. Moreover, computer simulations comparing the impact of Ar_{2000} and $(CO_2)_{2000}$ on an organic target illustrate that the CO_2 molecules remain intact during the trajectory and that the behavior of the CO_2 cluster on a molecular level is very similar to an atom of *m/z* 44. The advantages of using CO_2 cluster projectiles are shown to be related to the increased stability of the cluster itself and to the imaging resolution which is improved by more than a factor of 2. A consequence of this stability also allows the gas cluster ion source to be operated at much lower backing pressures.

These observations suggest that CO_2 clusters can be a viable projectile for imaging SIMS experiments, with several important advantages over existing commonly used probes.

Moreover, options still remain for taking advantage of the weak acidity of CO_2 to enhance ionization further perhaps by seeding with H_2O or HCl. In general, this platform provides a simple alternative to Ar - GCIBs that is straightforward to implement, inexpensive, and provides better SIMS image quality.

Supplementary Material

Refer to Web version on PubMed Central for supplementary material.

Acknowledgments

Financial support from the National Science Foundation (CHE-12-12645) and infrastructure support from the National Institutes for Health (grant number 5R01GM113746 – 22), and Novartis are gratefully acknowledged. DM and ZP would like to acknowledge financial support from the Polish National Science Center, grant numbers 2013/09/B/ST4/00094 and 2015/19/B/ST4/01892. We appreciate the assistance with sample preparation and AFM measurements by Dr. Jay Tarolli and Dr. Lars Breuer. Thanks to Prof. Andreas Wucher for the valuable comments on the paper.

References

1. Ninomiya S, Nakata Y, Honda Y, Ichiki K, Seki T, Aoki T, et al. A fragment-free ionization technique for organic mass spectrometry with large Ar cluster ions. Appl Surf Sci. 2008; 255:1588–1590.
2. Ninomiya S, Ichiki K, Yamada H, Nakata Y, Seki T, Aoki T, et al. Precise and fast secondary ion mass spectrometry depth profiling of polymer materials with large Ar cluster ion beams. Rapid Commun Mass Spectrom. 2009; 23:1601–1606. [PubMed: 19399762]
3. Rabbani S, Barber AM, Fletcher JS, Lockyer NP, Vickerman JC. TOF-SIMS with Argon Gas Cluster Ion Beams: A Comparison with C-60(+). Anal Chem. 2011; 83:3793–3800. [PubMed: 21462969]
4. Lee JLS, Ninomiya S, Matsuo J, Gilmore IS, Seah MP, Shard AG. Organic Depth Profiling of a Nanostructured Delta Layer Reference Material Using Large Argon Cluster Ions. Anal Chem. 2010; 82:98–105. [PubMed: 19957960]
5. Wehbe N, Mouhib T, Delcorte A, Bertrand P, Moellers R, Niehuis E, et al. Comparison of fullerene and large argon clusters for the molecular depth profiling of amino acid multilayers. Anal Bioanal Chem. 2014; 406:201–211. [PubMed: 24253407]
6. Sudraud P, Van De Walle J, Colliex C, Castaing R. Contribution of field effects to the achievement of higher brightness ion sources. Surf Sci. 1978; 70:392–402.
7. Levi-Setti R, Fox TR. High resolution scanning ion probes: Applications to physics and biology. Nuclear Instruments and Methods. 1980; 168:139–149.
8. Walker AV, Winograd N. Prospects for imaging with TOF-SIMS using gold liquid metal ion sources. Appl Surf Sci. 2003; 203:198–200.
9. Touboul D, Kollmer F, Niehuis E, Brunelle A, Laprevote O. Improvement of biological time-of-flight-secondary ion mass spectrometry imaging with a bismuth cluster ion source. J Am Soc Mass Spectrom. 2005; 16:1608–1618. [PubMed: 16112869]
10. Shard AG, Havelund R, Seah MP, Spencer SJ, Gilmore IS, Winograd N, et al. Argon Cluster Ion Beams for Organic Depth Profiling: Results from a VAMAS Interlaboratory Study. Anal Chem. 2012; 84:7865–7873. [PubMed: 22897795]
11. Matsuo J, Torii S, Yamauchi K, Wakamoto K, Kusakari M, Nakagawa S, et al. Novel SIMS system with focused massive cluster ion source for mass imaging spectrometry with high lateral resolution. Appl Phys Express. 2014; 7
12. Weibel D, Wong S, Lockyer N, Blenkinsopp P, Hill R, Vickerman JC. A C60 Primary Ion Beam System for Time of Flight Secondary Ion Mass Spectrometry: Its Development and Secondary Ion Yield Characteristics. Anal Chem. 2003; 75:1754–1764. [PubMed: 12705613]

13. Fletcher JS, Lockyer NP, Vaidyanathan S, Vickerman JC. TOF-SIMS 3D Biomolecular Imaging of Xenopus laevis Oocytes Using Buckminsterfullerene (C60) Primary Ions. Anal Chem. 2007; 79:2199–2206. [PubMed: 17302385]
14. Fletcher JS, Rabbani S, Henderson A, Lockyer NP, Vickerman JC. Three-dimensional mass spectral imaging of HeLa-M cells – sample preparation, data interpretation and visualisation. Rapid Commun Mass Spectrom. 2011; 25:925–932. [PubMed: 21416529]
15. Seah MP, Havelund R, Gilmore IS. Universal Equation for Argon Cluster Size-Dependence of Secondary Ion Spectra in SIMS of Organic Materials. J Phys Chem C. 2014; 118:12862–12872.
16. Sheraz née Rabbani S, Razo IB, Kohn T, Lockyer NP, Vickerman JC. Enhancing Ion Yields in Time-of-Flight-Secondary Ion Mass Spectrometry: A Comparative Study of Argon and Water Cluster Primary Beams. Anal Chem. 2015; 87:2367–2374. [PubMed: 25588151]
17. Sheraz née Rabbani S, Barber A, Fletcher JS, Lockyer NP, Vickerman JC. Enhancing Secondary Ion Yields in Time of Flight-Secondary Ion Mass Spectrometry Using Water Cluster Primary Beams. Anal Chem. 2013; 85:5654–5658. [PubMed: 23718847]
18. Berrueta Razo I, Sheraz S, Henderson A, Lockyer NP, Vickerman JC. Mass spectrometric imaging of brain tissue by time-of-flight secondary ion mass spectrometry – How do polyatomic primary beams C_{60}^+, Ar_{2000}^+, water-doped Ar_{2000}^+ and $(H_2O)_{6000}^+$ compare? Rapid Commun Mass Spectrom. 2015; 29:1851–1862. [PubMed: 26411506]
19. Wucher A, Tian H, Winograd N. A mixed cluster ion beam to enhance the ionization efficiency in molecular secondary ion mass spectrometry. Rapid Commun Mass Spectrom. 2014; 28:396–400. [PubMed: 24395507]
20. Tian H, Wucher A, Winograd N. Dynamic Reactive Ionization with Cluster Secondary Ion Mass Spectrometry. J Am Soc Mass Spectrom. 2016; 27:285–292. [PubMed: 26463238]
21. Tian H, Wucher A, Winograd N. Molecular imaging of biological tissue using gas cluster ions. Surf Interface Anal. 2014; 46:115–117. [PubMed: 26207076]
22. Angerer TB, Blenkinsopp P, Fletcher JS. High energy gas cluster ions for organic and biological analysis by time-of-flight secondary ion mass spectrometry. Int J Mass Spectrom. 2015; 377:591–598.
23. Lu C, Wucher A, Winograd N. Ionization effects in molecular depth profiling of trehalose films using buckminsterfullerene (C-60) cluster ions. Surf Interface Anal. 2011; 43:99–102.
24. Hill R, Blenkinsopp P, Thompson S, Vickerman J, Fletcher JS. A new time-of-flight SIMS instrument for 3D imaging and analysis. Surf Interface Anal. 2011; 43:506–509.
25. Garrison BJ, Postawa Z. Computational view of surface based organic mass spectrometry. Mass Spectrom Rev. 2008; 27:289–315. [PubMed: 18421766]
26. Liu L, Liu Y, Zybin SV, Sun H, Goddard WA. ReaxFF-lg: Correction of the ReaxFF Reactive Force Field for London Dispersion, with Applications to the Equations of State for Energetic Materials. J Phys Chem A. 2011; 115:11016–11022. [PubMed: 21888351]
27. Ziegler, JF.; Biersack, JP.; Littmark, U. The Stopping and Range of Ions in Solids. Pergamon; New York: 1985.
28. Aziz RA, Slaman MJ. The Argon and Krypton Interatomic Potentials Revisited. Mol Phys. 1986; 58:679–697.
29. Postawa Z, Czerwinski B, Szewczyk M, Smiley EJ, Winograd N, Garrison BJ. Enhancement of Sputtering Yields Due to C_{60} versus Ga Bombardment of Ag{111} As Explored by Molecular Dynamics Simulations. Anal Chem. 2003; 75:4402–4407. [PubMed: 14632043]
30. Czerwiński B, Samson R, Garrison BJ, Winograd N, Postawa Z. Desorption of organic overlayers by Ga and C_{60} bombardment. Vacuum. 2006; 81:167–173.
31. Plimpton S. Fast Parallel Algorithms for Short-Range Molecular-Dynamics. J Comput Phys. 1995; 117:1–19.
32. Tian H, Wucher A, Winograd N. Reduce the matrix effect in biological tissue imaging using dynamic reactive ionization and gas cluster ion beams. Biointerphases. 2016; 11:02A320.
33. Cheng J, Winograd N. Molecular depth profiling of multi-layer systems with cluster ion sources. Appl Surf Sci. 2006; 252:6498–6501.

34. Cheng J, Kozole J, Hengstebeck R, Winograd N. Direct comparison of Au_3^+ and C_{60}^+ cluster projectiles in SIMS molecular depth profiling. J Am Soc Mass Spectrom. 2007; 18:406–412. [PubMed: 17118671]

35. Wucher A, Cheng J, Winograd N. Molecular depth profiling of trehalose using a C60 cluster ion beam. Appl Surf Sci. 2008; 255:959–961.

36. Shen K, Wucher A, Winograd N. Molecular Depth Profiling with Argon Gas Cluster Ion Beams. J Phys Chem C. 2015; 119:15316–15324.

37. Toyoda N, Yamada I. Gas cluster ion beam equipment and applications for surface processing. IEEE T Plasma Sci. 2008; 36:1471–1488.

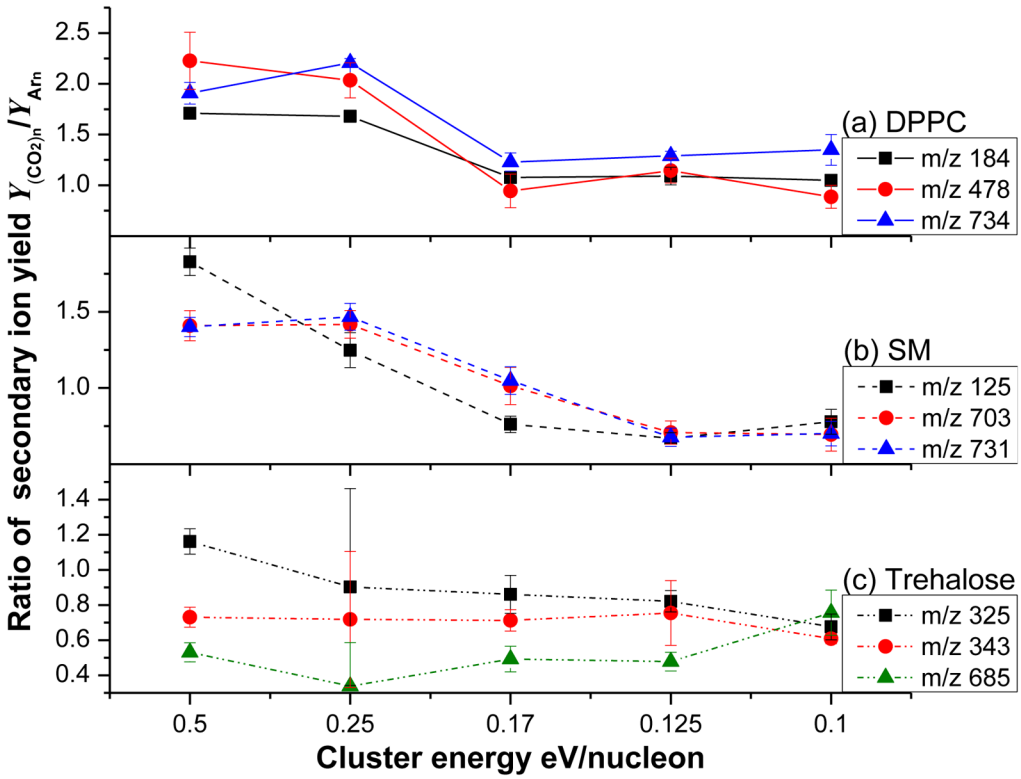

Figure 1.

The ratio of selected secondary ion yields along with a series of $(CO_2)_n^+$ and Ar_n^+ clusters from DPPC in (a), SM in (b) and trehalose in (c). A value of unity implies the secondary ion intensity associated with each ion is identical. The cluster impact energy is reported in energy per nucleon so that the properties of clusters with the same mass can be compared directly. Here the cluster size increases from 1000 to 5000 particles as the energy/nucleon decreases from 0.5 to 0.1.

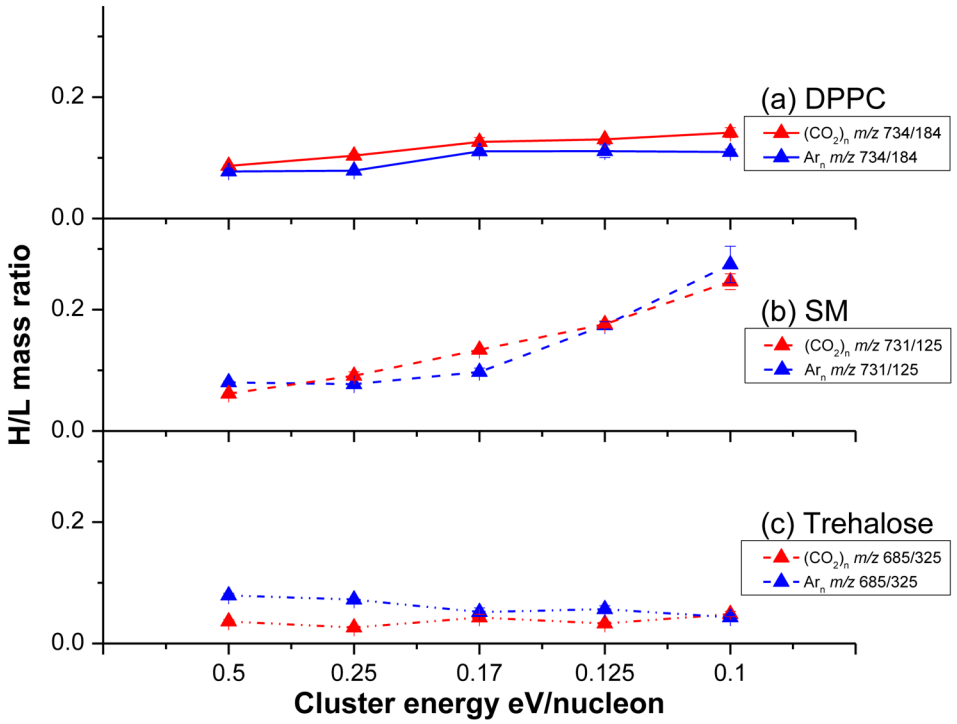

Figure 2.

The H/L mass ratio (selected high mass ions to major fragment) for $(CO_2)_n^+$ and Ar_n^+ bombardment of DPPC in (a), SM in (b) and trehalose in (c). The cluster energy is reported in energy per nucleon so that the properties of clusters with the same mass can be compared directly. Here the cluster size increases from 1000 to 5000 particles as the energy/nucleon decreases from 0.5 to 0.1.

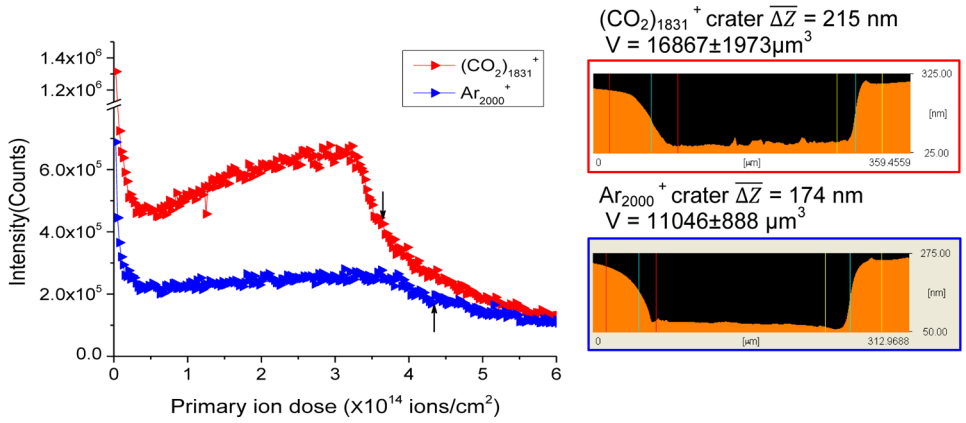

Figure 3.

Sputter depth profiles of a trehalose film using Ar_{2000}^{+} and $(CO_2)_{1831}^{+}$, respectively. Arrows indicate the interface between trehalose and the silicon substrate. The AFM images of the crater produced by each projectile are also shown. Note that the film thickness is slightly different for each case.

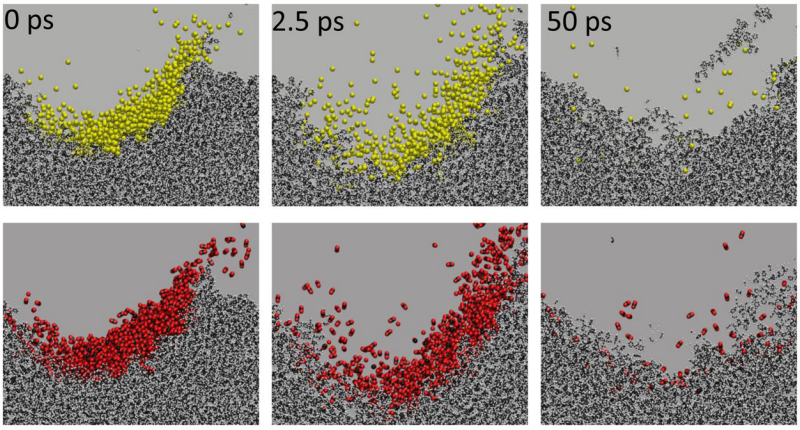

Figure 4.

Comparison of molecular dynamics computer simulations of 20 keV Ar_{2000} (top 3 panels) with $(CO_2)_{2000}$ (bottom 3 panels) bombarding a polystyrene substrate at 45° angle of incidence. The time evolution, from 0 ps to 50 ps is noted in the figure. Colors are as follows: argon is yellow, carbon is black, oxygen is red and hydrogen is gray. See text for details about the computation. Note that the evolution of the trajectory proceeds in a very similar fashion for both projectiles, and that no CO_2 molecules are observed to fragment in the first 50 ps.

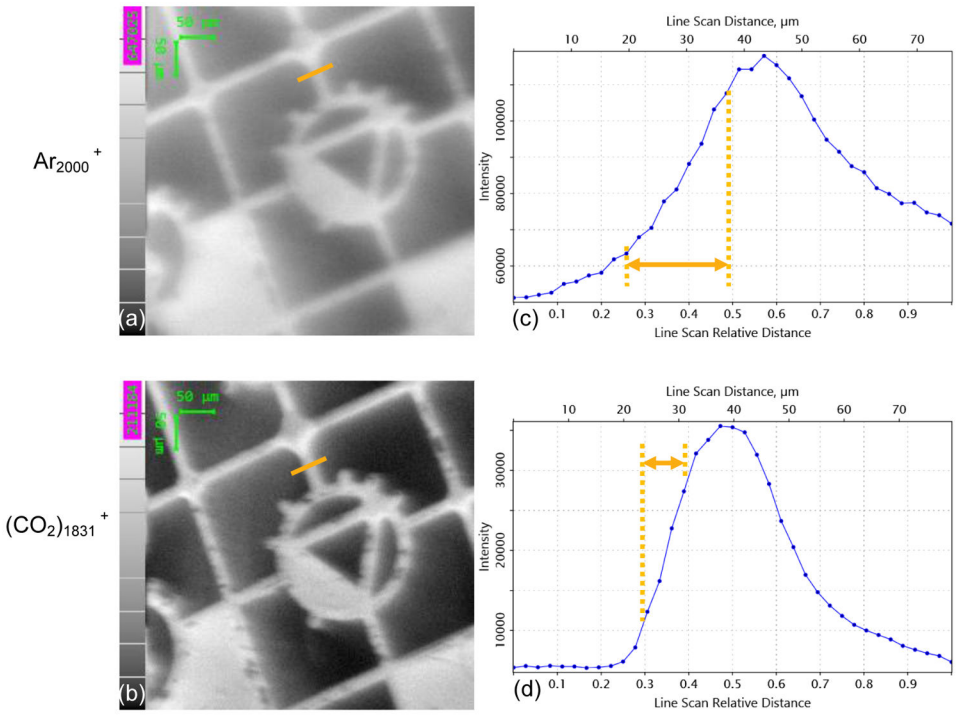

Figure 5.

Imaging of a rubrene - coated grid with Ar_{2000}^{+} and $(CO_2)_{1823}^{+}$. A line scan across on of the grid bars indicated by the orange line was utilized to determine the beam focus of Ar_{2000}^{+} and $(CO_2)_{1831}^{+}$ respectively. The 20 – 80 % intensity difference is indicated on the graph.